DCT-Tensor-Net for solar flares detection on IRIS data

Denis Ullmann*, Slava Voloshynovskiy*, Lucia Kleint†, Sam Krucker†,
Martin Melchior†, Cédric Huwyler†, Brandon Panos†

* *CUI - SIP*
UNIGE
Geneva, Switzerland

† *I4DS*
FHNW
Windisch, Switzerland

denis.ullmann@unige.ch, svolos@unige.ch, lucia.kleint@fhnw.ch, krucker@ssl.berkeley.edu,
martin.melchior@fhnw.ch, cedric.huwyler@fhnw.ch, brandon.panos@fhnw.ch

***Abstract*—Flares are an eruptive phenomenon observed on the sun, which are major protagonists in space weather and can cause adverse effects such as disruptions in communication, power grid failure and damage of satellites. Our method answers the importance of the time component in some scientific video observations, especially for flare detection and the study is based on NASA's Interface Region Imaging Spectrograph (IRIS) observations of the sun since 2013, which consists of a very asymmetrical and unlabeled big data. For detecting and analyzing flares in our IRIS solar video observation data, we created a discrete cosine transform tool DCT-Tensor-Net which uses an empirically handcrafted harmonic representation of our video data. This is one of the first tools for detecting flares based on IRIS images. Our method reduces the false detections of flares by taking into consideration their specific local spatial and temporal patterns.**

***Index Terms*—big data applications, computer aided analysis, scientific computing, data processing, data analysis, data preprocessing, feature extraction, image texture analysis, detection algorithm, discrete cosine transforms, astrophysics.**

I. Introduction

Modern astronomical observations produce thousands of terabytes of data on a daily basis. The important aspect of these data can no longer be analyzed manually. Astronomers therefore face many difficult yet common situations for analyzing, understanding and extracting models from the observations of complex and unexplained phenomena. They often have to face not labeled big data, where classical machine learning may fail to detect and analyze the data with high accuracy.

In our proposed method we use video observations of the sun produced by recent IRIS NASA's Interface Region Imaging Spectrograph, developed and operated by LMSAL [1]. The challenge is to detect the apparition of solar flares automatically in the IRIS videos, which are the result of the reconfiguration of the magnetic field in the corona. Flares are considered to be major protagonists in space weather and can cause adverse effects on the Earth such as disruption in communications, power grid failure and damage of satellites.

We propose a tool for flare detection and analysis of IRIS videos, based on a video tensor harmonic analysis, by composing time component discrete cosine transform (1D-DCT) with spatial discrete cosine transform of the images (2D-DCT). Other methods for the detection of solar flares have been achieved for other types of data collected by ground and space based observations. These methods use, amongst others: a derivative threshold of the pixel value for SoFAST, the flare detector of PROBA2/SWAP satellite [2], by thresholding the differences of frames partitioned in local blocks for Hinode FLare Detector tool [3], by specific conditions on the 6-12 keV count-rate timelines and its local temporal derivatives for the RHESSI Flare finder [4], again by thresholding the derivative of the macropixel value lightcurve for the SDO Flare Detective, by hand-crafted intensity levels detections on Solar Demon detector [5], by neural networks [6] and support vector machines [7] or thresholding based on the geometry of the histogram [8]. Yet these methods are from full-disk observations or even by combining different observations of the full disk, with much simpler observational modes than IRIS. In contrast, IRIS's multiple observational modes (see [2], table 12, 13 & 14) motivates us to propose a method, which allows physical analysis of the flares in addition to their detection in the big data collected *on fly*. We present the first method able to separate the space of IRIS data for extracting and analyzing the class of flares.

We point out that our data are very asymmetric and not labeled at this point, that leads to difficulties for quantifying the accuracy of our method at this stage. We could estimate that there are about 400 flares in our observations of IRIS

Project #407540_167158 supported by SNSF - NRP75 Big Data

data since 2013 (see [9], this list is subjected to corrections). Our testing dataset contains about forty flaring and non-flaring observations discovered according to the appendix of [10]. The possibility of automatic detection of flares in IRIS images is highly demanded by IRIS community and would be a useful tool for extensive analysis of flares [10], [11]

Our detection method is a handcrafted DCT Tensor Network, which allows to capture time and spatial frequency patterns in the first layer. We choose to decompose our videos in the spatial frequency domain with DCT because of its logarithmic complexity compared to other tensor analysis tools. It also allows astronomers to extract frequency features for further analysis. We empirically selected the frequencies responsible for the flaring observations. At this stage, this frequency selection is empirical and hence fully supervised and likely not optimal but good enough to detect flares as we finally show relevant results on the data that we tested (see IV-A): the totality of the flares tested are detected and the sequences without flares are all rejected except in the very special case of limb observation, this special case should be solved with a future evolution of our method that we describe on IV-A.

As far as we know, our video processing approach is new and we are on the merge to release a public python package for DCT-Tensor-Net analysis.

II. Presentation

A. Solar flares and IRIS satellite

In 1859 the first and largest flare ever observed was seen by Carrington with the naked eye and 17 hours after the flash it reached the Earth, causing many strong adverse effects such as massive northern lights, temporary inversion of the resulting magnetic field of the Earth and electrocution of telegram messengers. Solar flares are major protagonists in space weather and can cause adverse effects such as disruption in communications, power grid failure and damage of satellites. They are the result of the reconfiguration of magnetic fields in the corona. These energetic events accelerate highly energetic particles into space and toward the solar surface, where they cause heating and emission in a broad range of wavelengths. The sun is following a cycle [12] and a similar super flare could appear soon, now about 150 years after Carrington's flare. It's a big concern to be able to detect, understand and predict flares.

The solar observation data collected by NASA's IRIS satellite may bring us a big advance for this purpose. The IRIS investigation combines advanced numerical modeling with a high resolution UV imaging spectrograph with a data-rate of 0.7 Mbits/s. Since its launch, it has collected a few tens of terabytes of data, including a multitude of flares.

Our method only focuses on the time sequences of the slit-jaw images (SJI) [2]. These are video records of only pre-selected regions of the sun and with a wide variety of recording settings (see [2], table 12, 13 & 14). The analysis based on the images will be later combined with the analysis based on the spectral observations. We want to highlight that the videos observed correspond to special wavelengths in the UV domain with four possibilities: 1330, 1400, 2796 and 2832 A, and it is not possible to do multiple wavelengths observation at the same time.

B. Data description and detection challenge

We work with the level 2 IRIS data [13], which provide pre-processed observation videos with almost well aligned frames but may have few pixels of misalignment. Perfect alignment of the information between frames is also not possible on limb observation and because of the complex underlying geometry due to the mutual dynamics of the Sun and the satellite. The data may also be very noisy or contain over-saturated or missing values caused by cosmic rays and dust particles respectively.

We accumulate about 8 terabytes of raw data per year since 2013, but we estimate that less than the thousandth of this data are flares. Our data are asymmetric and also not labeled, which oriented us toward unsupervised or semi-supervised methods. We present a hand-crafted method, which can be interpreted as a DCT Tensor Network that is reducing the size of the input video tensor by harmonic decomposition of the signal, empirically selecting a range of frequency domains for flare detection. This method is a straightforward handcrafted Network for which all available data is used for testing and for the empirical selection of the frequency domain for flare detection. Finally, we produce an output of classifier indicating the probability of flare observation.

We present the first tool for flare detection on IRIS data and that may also be a support for further labeling and analysis of the flares.

C. Visualization of the results

Some videos of our results are available at the web site of our project [14] and [15].

The harmonic analysis decomposition of the video tensor is applied on groups of 10 successive frames with an overlap of 5 frames of these analysis such that each frame except the 5 first and the 5 or less remaining last frames of the video is included in exactly two groups : one representing "the past" and another representing "the future" of the current frame. The histogram is shown to see that the IRIS data are more complex that what has been done in [8]. See Fig. 1 for a descriptive explanation of the frames :

$\boldsymbol{IMG}$: The current image,
$\boldsymbol{Hist}$: The current histogram,
DCT_a : The DCT analysis of the ending sequence,
$\boldsymbol{FP_a}$: The corresponding flare appearance probability on the global image,
DCT_b : The DCT analysis of the beginning sequence,
$\boldsymbol{FP_b}$: The corresponding flare appearance probability on the global image.

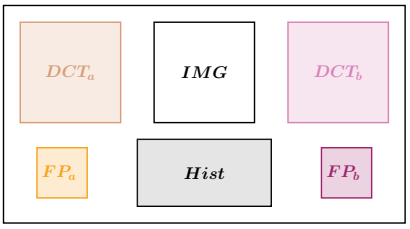

Fig. 1. Frame organization for visualization of the results.

III. Proposed approach

A. Justification

The time component is a very important parameter for flare detection, it is used in most of the other flares detection methods (see [2], [3], [4], [5], [6], [7], [8]) through derivatives or successive frames subtractions and even for astronomy experts, it may become difficult to certify on a single image if there is a flare or not. Looking at our data in the frequency domain gives many advantages, for physical feature extraction and for a time component analysis.

Firstly we represent all the images of our video tensor in the frequency domain by applying a 2D DCT to each frame. It results in perfectly aligned frames in the spatial frequency domain that one can more easily compare.

Secondly, thanks to this perfect alignment, we apply a 1D DCT for all pixels with respect to the time component and we flatten our data by keeping only the variance of the result. This produces an estimate of the time variations in the spatial frequency domain of our data. Such a harmonic analysis should be suitable for detecting the changes due to flares.

Computing DCT has a logarithmic complexity and present then great advantages comparing to other tensor analysis in a context of big data.

B. Notations and conventions

For the following III-C, III-D, III-E, III-F sections, we use the following notations:

Bold capital letters are used for functions fully representing their data with all their variables, we call them full functions, whereas italic capital letters are restrictions of full functions. For example, in our situation, a video is a full function and has 3 variables because it is a tensor of dimension 3, whereas frames of this video are restrictions of this full function, they have 2 variables whereas they are in a 3 dimensional space. We note:

$$\begin{gathered}\mathbf{I} : (x, y, t) \mapsto \mathbf{I}(x, y, t) \quad \text{(video } \mathbf{I}\text{)} \\ I(\cdot, \cdot, t) : (x, y) \mapsto I(x, y, t) \quad \text{(frame } t\text{)}\end{gathered}$$

We use the following notations for the 1D DCT:

$$\mathbf{K}(u, v, \theta) = DCT_t\left(\mathbf{J}(u, v, t)\right)$$

$$= \frac{c(\theta)}{\sqrt{T}} \sum_{t=0}^{T-1} \mathbf{J}(u, v, t) f_T(t, \theta), \tag{1}$$

where $f_T(t, \theta) = \cos\left(\frac{(2t+1)\theta\pi}{2T}\right)$. And for the 2D DCT:

$$\mathbf{J}(u, v, t) = DCT_{x,y}\left(\mathbf{I}(x, y, t)\right)$$

$$= \frac{c(u)c(v)}{\sqrt{XY}} \sum_{\substack{x=0 \\ y=0}}^{\substack{X-1 \\ Y-1}} \mathbf{I}(x, y, t) f_X(x, u) f_Y(y, v), \tag{2}$$

where $c(u) = \sqrt{2}$ if $u \neq 0$ and $c(0) = 1$.

We also use the following notations for the partial variances:

$$Var_\theta\left(\mathbf{K}(u, v, \theta)\right) = \mathbf{E}\left[K(u, v, \cdot)^2\right] - \mathbf{E}\left[K(u, v, \cdot)\right]^2, \tag{3}$$

where (u, v) are coordinates in the spatial frequencies domain and and θ is the coordinate in the time frequencies domain.

$$Var_{(u,v)\in\mathbf{DL}}\left(\mathbf{L}(u, v)\right) = \mathbf{E}_{(u,v)\in\mathbf{DL}}\left[\mathbf{L}^2\right] - \mathbf{E}_{(u,v)\in\mathbf{DL}}\left[\mathbf{L}\right]^2,$$

where $\mathbf{L}$ is an image in the spatial frequencies domain and $\mathbf{DL}$ is a selected sub-domain for the spatial frequencies coordinates of $\mathbf{L}$ and:

$$\mathbf{E}_{(u,v)\in\mathbf{DL}}\left[\mathbf{L}\right] = \frac{1}{|\mathbf{DL}|} \sum_{(u,v)\in\mathbf{DL}} \mathbf{L}(u, v).$$

C. 3D DCT

The 3D DCT explained in the "Fig. 2" is applied locally on portions of the video tensor of size $20 \times 20 \times 10$.

D. Selection of the discriminating part

In this section, we give some explanations about the hand-crafted selection of the discriminating sub-domain $\mathbf{DL}$ which corresponds to step **S** in the Fig. 2.

After obtaining different frequency local patterns we compare the ones coming from portions in flare regions to the rest of the profiles and we try to identify a sub-domain of the spatial frequency domain where the profiles behave differently in the regions of flares. Fig. 3 shows few examples about how we decided to select only the central part of the profiles and we compute then the sub-domain variance. Of course there are many more different profiles but we tried to manually find a general behavior.

E. Decomposition of the cube

The full video tensor is partitioned as shown in Fig. 5 into small data cubes of size $20 \times 20 \times 10$ such that the partition cover all the video with a time-component overlapping of 5 frames. All these small data cubes are flattened by the 3D DCT of section III-C.

The dimensions of the small data cubes are chosen empirically and correspond to the precision of detection that we want to have on our image.

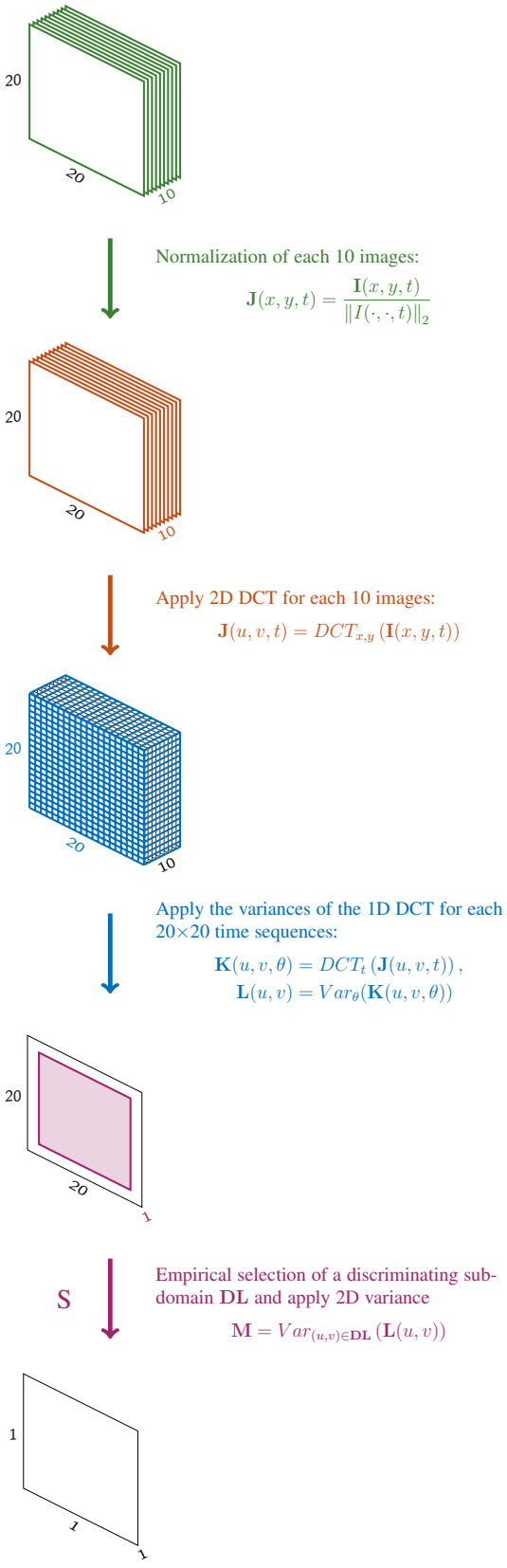

Fig. 2. Description of the 3D DCT.

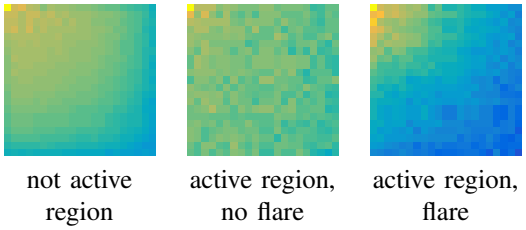

Fig. 3. Visualization of possible outputs of the 3D DCT.

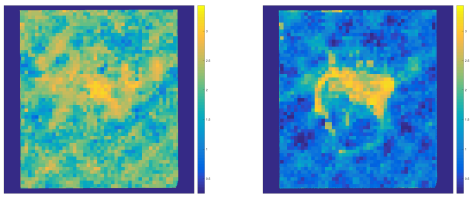

Fig. 4. Visualization of some outputs of the 3D DCT.

F. Global probability of flare appearance

Fig. 5 shows that we tuned a probability function for the global flare appearance on the image from the results of all 3D-DCTs applied on all video. It appeared that when a flare happens in the image, the global contrast of the result increases drastically as shown in Fig. 4. We compute the flaring output probability as a function of the variance of all values of a sequence obtained after our 3D-DCT and frequency selection. We used Popoviciu's inequality [16] and the Von Szokefalvi Nagy inequality [17] which state that if M and m are the upper and lower bounds on the values of any random variable X with a particular probability distribution, and if the sample size is finite, then:

$$m_{Var} = \frac{(M-m)^2}{2n} \leq Var(X) \leq \frac{(M-m)^2}{4} = M_{Var},$$

where n is the sample size, and by constraining our function on its derivative values at its extremums, we defined the flaring output probability as follows:

$$p_{flare}(Var_{sd}) = \frac{\sqrt{Var_{sd}}}{M_{Var} - m_{Var}} \sin \frac{\pi\sqrt{Var_{sd}}}{2(M_{Var} - m_{Var})},$$

where sd stands for the selected subdomain in III-D. Actually, as Popoviciu's equality holds exactly when half of the probability is concentrated at each of the two bounds, we tuned this function by considering 2.5 times of this formula if it outputs a value smaller then 1. Therefore, the probability function for the global image appearance of a flare is tuned by taking the global variance on the whole image and by mapping it between 0 and 1.

For the visualization, the blue color corresponds to a zero probability of flare appearance and the yellow color corresponds to the highest probability of flare appearance.

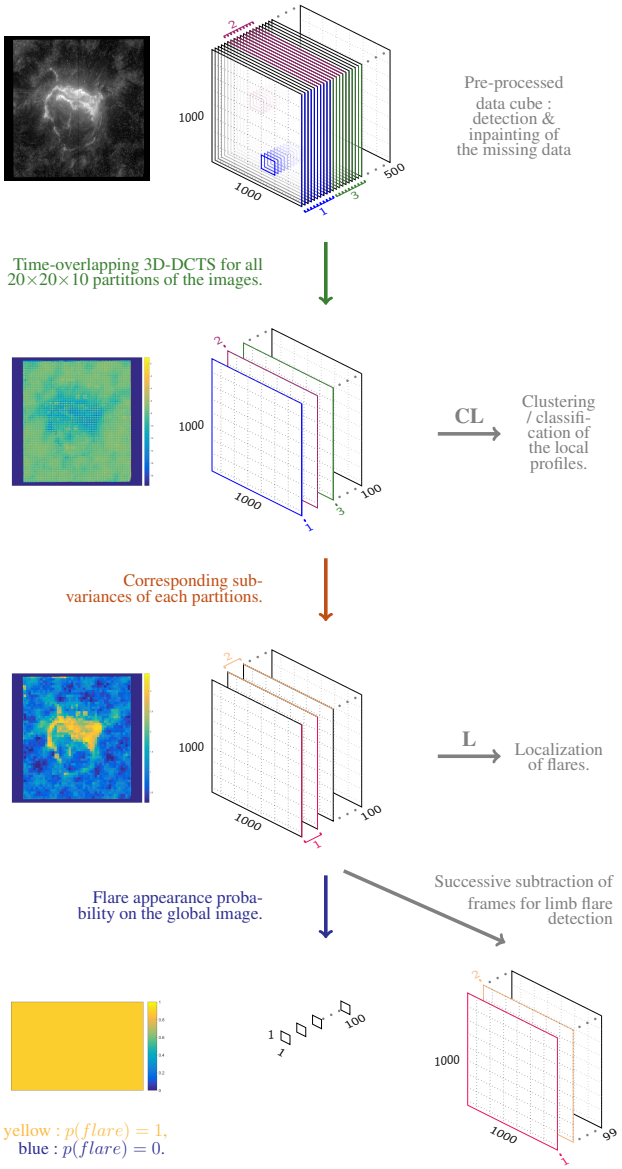

Fig. 5. Detection and analysis on the full data cube.

IV. Computing Simulations

A. First results

Some videos of our results are available at the internet site of our project [14], [15]. As we mentioned in section II-B, our unlabeled data are very asymmetric. We estimate that we have only about 400 flare in our data from the daily observation since 2013. This small amount of flares leads to restrictions of using deep learning methods trained on flares and motivates the favor of hand-crafted approach. Fig. 6 shows the confusion matrix and accuracy of our results on 784 sequences of 10 frames (see section III-E and Fig. 5) corresponding to no-limb and 1400A observations. It represents 16.5GB of the 50TB of data.

This shows that we have a 99.8% accuracy for the detection on these 784 sequences. The flare that was not detected was

detection	true flare	true no-flare
flare	43	0
no-flare	1*	740

Fig. 6. Confusion matrix on the sequences of 10 consecutive frames.

* The flare is present only in the first frame of video.

actually appearing only on the first frame of the video so our method could hardly detect it at this stage as it gives importance to the evolution in time. As shown in Fig. 5 on step C', we prepare improvements for our method, firstly for the special case of limb observations by subtracting consecutive flares. We could also use border detection methods.

We have for now only this list of labeled data so the number of results will grow in future with more labeled data inputs from the astronomers experts. We wish that our detector will help to produce a quite bigger labeled dataset in order to apply machine learning to IRIS dataset.

B. Pre-processing

Before proceeding with the 3D-DCT analysis, the data cube is pre-processed with a border missing data extraction and an in-painting of the missing data. The pre-processing shows high performance for any small area of missing data, and also for large areas if there is information nearby in time at the given location. The missing data is recovered by all the information contained in the video data-cube, being firstly initialized to the values of the 3D nearest neighbors and then by recursive smoothing (see [18]).

By experience, forty iterations are enough to get good quality data (see Fig. 7 comparing with classic IRIS dust-remover tool**) and our method gives much more reliable results after this pre-processing.

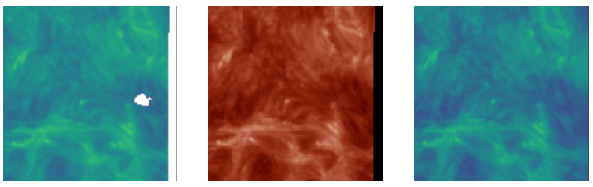

Fig. 7. Quality of pre-processing.

C. Development

Our tool will have soon new updates: the first one will be the localization of the flares in image once they are detected (step L in Fig. 5), and the second one will provide a clustering or a classification of the local DCT profiles (step CL in "Fig. 5"). These two developments show that our tool is not only available for flare detection but also for analyzing them as the frequency domain seams to be suited for working on the solar flares.

Also, we are on the merge to release a public python package for these methods.

V. Conclusion

We propose a new method for detecting and analyzing flares on IRIS NASA's Interface Region Imaging Spectrograph, beginning with pre-processing the data with missing values by inpainting, following by converting the images into the spatial frequency domain. In this way our images are well aligned and we proceed to another step of frequency analysis applied on the time component. This gives us information on the variations in the spatial frequency domain with respect to the time component. Thanks to this visualization we found out the frequency sub-band with the best distinguishability between flares and non-flares. Even if we didn't had enough labeled data in order to train and make optimal the frequency selection, the results are good. One of the advantage of this method is its fast logarithmic complexity and it is therefore much pertinent in a context of Big Data.

When we apply it to all regions of an IRIS observation video of the sun, the flaring sequences appear quite different from the rest. This allow us to tune a global sequence probability of flare detection, and will also allow us to localize flares on the image and classify or cluster them.

With our DCT-Tensor-Network we made the first tool able to detect flares in IRIS images data and we believe that this structure could be useful for other scientific video observations analysis. We also hope that it will help us to label the big data of IRIS observations. The classification or clustering results of our method should be subjected to future cross-validation and correlation with the analysis made from the spectral data of IRIS [1] in order to understand better the solar flare phenomenon.

Acknowledgment

Many thanks to LMSAL & NASA for having allowed us to download all the IRIS data from their servers and to Olga Taran (UNIGE - SIP) for her precious image processing advises.

References

[1] B. De Pontieu et al., "The interface region imaging spectrograph (IRIS)", Springer, Solar Physics, SOLA: iris_mission_final.tex; 21 January 2014; 15:18, DOI:10.10007, 2014.

[2] K. Bonte, D. Berghmans, A. De Groof, K. Steed, S. Poedts, "SoFAST: automated flare detection with the PROBA2/SWAP EUV Imager", Springer, Solar Pys (2013) 286:185-199, DOI 10.1007/s11207-012-0165-8, 2012.

[3] Kano et al., "The Hinode X-ray telescope (XRT): camera design, performance and operations", Solar Phys. 249,263-279, doi: 10.1007/s11207-007-9058-7, 2008.

[4] Lin et al., "The Reuven Ramaty high-energy solar spectroscopic imager (RHESSI)", Solar Phys. 210, 3-32. doi:10.1023/A:1022428818870, 2002.

[5] P. Grigis, A. Davey, P. Martens, P. Testa, R. Timmons, Y. Su, SDO feature finding team, "The SDO flare detective", Bull. Am. Astron. Soc. 41, 874, 2010.

[6] Roberto A. Fernandez Borda, Pablo D. Mininni, Cristina H. Mandrini, Daniel O. Gmez, Otto H. Bauer, Marta G. Rovira, "Automatic Solar Flare Detection Using Neural Network Techniques", Solar Pys, April 2002, Volume 206, Issue 2, pp 347357, 2002

[7] Ming Qu, Frank Y. Shih, Ju Jing, Haimin Wang, "Automatic solar flare detection using MLP, RBF and SVM", Solar Physics 217: 157172, 2003.

[8] C. Caballero, M. Aranda, "Automatic tracking of active regions and detection of solar flares in solar EUV images", Sol. Phys., 289 (5), 16431661, DOI: 10.1007/s11207-013-0415-4, 2014.

[9] Kathy Reeves, Jakub Prchlik, Hui Tian, Ying Li, "IRIS flare list", http://pyoung.org/iris/iris_flare_papers.html, 2018.

[10] Panos et al., "Identifying Typical MG II Flare Spectra Using Machine Learning", The Astrophysical Journal, 2018

[11] Butler et al. 2018, American Astronomical Society Meeting Abstracts #232, 232, #121.01

[12] David H. Hathaway, "The solar cycle", Springer, Living reviews in solar physics, 2015.

[13] Tiago M. D. Pereira et al., "A users guide to IRIS data retrieval, reduction & analysis", release 1.0, LMSAL, 2018.

[14] bigastro.unige.ch

[15] www.youtube.com/channel/UC0na1JK7aEGXmlXe8XJxmZQ

[16] Popoviciu, "Asupra ecuaiilor algebrice care au toate rdcinile reale", Mathematica (Cluj). 9: 129145, 1935.

[17] Nagy JVS, "Uber algebraische Gleichungen mit lauter reellen Wurzeln", Jahresbericht der deutschen mathematiker-Vereingung, 27:3743, 1918.

[18] Damien Garcia, "Robust smoothing of gridded data in one and higher dimensions with missing values", Computational Statistics and Data Analysis 54 (2010) 11671178, & http://www.biomecardio.com/matlab/inpaintn_doc.html, 2009